Banner appropriate to article type will appear here in typeset article

The motion of a surfactant-laden bubble in a channel or a Hele-Shaw cell

- D. J. Booth^{1,2}, I. M. Griffiths ²†, P. D. Howell²†
- ¹Mathematics Institute, University of Warwick, Coventry CV4 7AL, UK
- ²Mathematical Institute, University of Oxford, Andrew Wiles Building, Oxford, OX2 6GG, UK
- (Received xx; revised xx; accepted xx)
- We investigate how the addition of surfactant affects the governing equations for a bubble in a 7
- two-dimensional channel in the small-capillary-number limit. In the limit where the timescale 8
- for absorption of surfactant is much shorter than the timescales for transport of surfactant 9
- along the surface of the bubble, we derive a set of idealised free-surface boundary conditions 10
- that capture the effects of surfactant in a single dimensionless "elasticity parameter", and 11
- apply them to the front and rear of the bubble separately. At the front of the bubble, there 12
- are three regions of interest: the front cap, the thin film region, and a transition region that 13
- smoothly connects the other two regions. Through matched asymptotic expansions, we derive 14
- predictions for the thin film height and the pressure drop across the front meniscus. We find 15
- that the viscous pressure drop across the front meniscus is always larger for a surfactant-16
- laden bubble than for a surfactant-free bubble, by an order-one factor of up to $4^{2/3}$. Using 17
- a similar analysis at the rear of the bubble, we find that the viscous pressure drop across 18
- the rear meniscus is also always larger in magnitude for a surfactant-laden bubble than for a 19
- surfactant-free bubble, again up to a maximum factor of $4^{2/3}$. Finally, we use these results to 20
- show that, for the same flow conditions, an isolated surfactant-laden bubble in a Hele-Shaw
- 21
- cell will travel more slowly than an isolated surfactant-free bubble. 22

1. Introduction 23

- Bretherton (1961) first analysed the motion of a surfactant-free bubble through a viscous 24
- liquid in a capillary tube. His analysis was modernised by Park & Homsy (1984) into the 2.5
- language of matched asymptotic expansions. We follow a similar methodology in this paper 26
- for a surfactant-laden bubble. We then use the results of the analysis to show how the equation 27
- of motion derived by Booth et al. (2023) for an approximately circular bubble in a Hele-28
- Shaw cell is modified by the presence of surfactant, resulting in a model that systematically 29
- accounts for the effects of surfactant-laden thin liquid films above and below the bubble, 30
- without the inclusion of any ad hoc fitting paramters. 31
- There is a plethora of literature studying the propagation of a bubble or a finger of 32
- air in a viscous liquid containing surfactants (see, for example, Ghadiali & Gaver 2003; 33
- Halpern & Gaver 2012; Park 1992; Ratulowski & Chang 1990; Stebe & Barthes-Biesel 34
- 1995, and references therein). In particular, Ratulowski & Chang (1990) extended the 35
- results of Bretherton (1961) to a finger of air propagating into a viscous liquid containing

[†] Email address for correspondence: ian.griffiths@maths.ox.ac.uk, howell@maths.ox.ac.uk

soluble surfactants. They proposed five different distinguished limits based on the convective, diffusive and kinetic timescales. Park (1992) built on the work of Ratulowski & Chang to consider the flow of a long bubble in a capillary tube and found that surfactants can rigidify the bubble's surface. Maruvada & Park (1996) used these results to describe a rigid elliptical surfactant-laden bubble in a Hele-Shaw cell, generalising the Taylor & Saffman (1959) solution for the motion of a bubble with constant Laplace pressure to include the rigidifying effects of surfactants that can occur in the "convective equilibrium" regime proposed by Ratulowski & Chang (1990).

In this paper, we focus on what Ratulowski & Chang term the "bulk equilibrium" model, in which there is an abundance of surfactant in solution, such that the bulk concentration remains approximately constant. Physically, this limit could correspond to the bulk surfactant concentration being significantly above the critical micelle concentration (CMC). Furthermore, we consider the regime in which the surfactant is highly soluble, so the surface concentration is close to equilibrium with the bulk. Such a system has been recently studied experimentally by Baué *et al.* (2025). While the work we present in this paper is focused on the motion of a bubble, the methodology can be adapted to study the propagation of a liquid plug or film coating. This problem thus has applications also to the transport of fluid in the lung (see Waters & Grotberg 2002; Halpern & Gaver 2012; Shemilt *et al.* 2023; Grotberg 2011), and in fibre coating (see Shen *et al.* 2002; Delacotte *et al.* 2012).

Ginley & Radke (1989) also study a surfactant-laden bubble in a capillary tube, while Waters & Grotberg (2002) study the similar problem of the propagation of a surfactantladen plug. Both of these papers investigate a regime where the surfactant concentration is close to equilibrium, with the resulting Marangoni stress along the bubble interface being negligible at leading order. Both then provide asymptotic results for the pressure drop across the propagating bubble or plug and the height of the thin film deposited behind. We consider a similar regime in this paper; however, we study the distinguished limit in which Marangoni effects enter the problem at leading order. In the limit of small Marangoni stress we recover the asymptotic predictions of Waters & Grotberg (2002) and Ginley & Radke (1989); however, we find that their prediction that the film height decreases with increasing Marangoni stress quickly fails. The thin film height actually starts to increase as the strength of the Marangoni effect is increased, to a maximum factor of $4^{2/3}$ times the Bretherton prediction for a surfactant-free bubble. The factor $4^{2/3}$ has been seen in multiple studies of large Marangoni stress (see, for example, Ratulowski & Chang 1990; Park et al. 1994; Stebe & Barthes-Biesel 1995; Shen et al. 2002), and occurs due to the bubble surface being stationary in the lab frame of reference, rather than satisfying the zero-stress condition used in the original Bretherton problem.

The basic problem studied in this paper consists of a surfactant-laden bubble propagating along a two-dimensional channel, as sketched in figure 1. For the surfactant-free case, Bretherton (1961) obtained approximate formulae for the height \hat{h}_{∞} of the thin film deposited by the front meniscus and the pressure drop $\hat{p}_b - \hat{p}$ across the bubble meniscus, in the limit as the capillary number Ca tends to zero, namely

$$\hat{h}_{\infty} \sim a \,\hat{H} \,\mathrm{Ca}^{2/3} \tag{1.1}$$

79 and

$$\hat{p}_b - \hat{p} \sim \frac{\hat{\gamma}_0}{\hat{H}} + \beta \frac{\hat{\gamma}_0}{\hat{H}} \operatorname{Ca}^{2/3}. \tag{1.2}$$

The dimensionless prefactors a and β are determined numerically: $a \approx 1.337$, while the

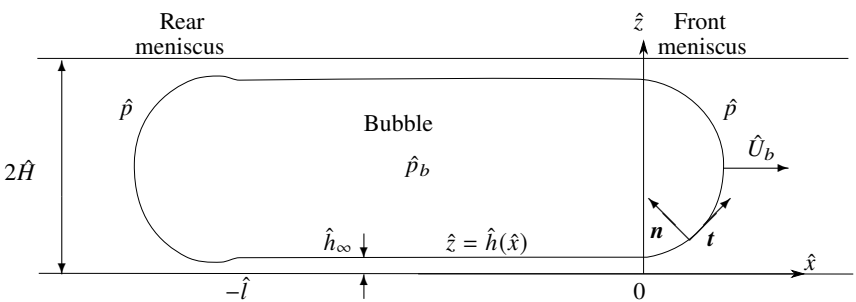


Figure 1: Schematic of a two-dimensional surfactant-laden bubble propagating at speed \hat{U}_b along a channel of height $2\hat{H}$. We take the origin to be at the start of the thin film region, whose length and height are denoted by \hat{l} and \hat{h}_{∞} , respectively. The pressures in the bubble and in the fluid outside are denoted by \hat{p}_b and \hat{p} , respectively.

value of β depends on whether the meniscus is advancing or retreating, with

83
$$\beta = \begin{cases} \beta_1 \approx 3.88 & \text{at front (advancing) meniscus,} \\ \beta_2 \approx -1.13 & \text{at rear (retreating) meniscus.} \end{cases}$$
 (1.3)

Our aim in this paper is to determine how the values of these constants $\{a, \beta_1, \beta_2\}$ are modified for a surfactant-laden bubble, using systematic matched asymptotic expansions. We then apply these results to the propagation of a surfactant-laden bubble through a Hele-Shaw cell and thus derive a drag law that contains no *ad hoc* fitting parameters, in a similar fashion to Booth *et al.* (2023).

This paper is structured as follows. We begin in §2 by writing down the governing equations for the flow around a bubble propagating through a two-dimensional channel containing a surfactant-laden viscous liquid. In §3 we describe the asymptotic structure of the front region of the bubble, following the methodology of Park & Homsy (1984). We find that there are three regions of interest: the front cap, the thin film region, and the transition region, which allows for a smooth transition from the front cap into the thin film region. The equations in the transition region are then analysed in §4, whereby we find the surfactant-laden analogues of a in (1.1) and β_1 in (1.3). In §5 we describe the asymptotic structure of the rear of the bubble, which has an additional matching condition that the height \hat{h}_{∞} of the thin film flowing towards the rear of the bubble must equal the height of the thin film deposited by the front meniscus. Then, in §6, we analyse the rear transition region to find the surfactant-laden analogue of β_2 in (1.3). Combining the results of §§4 and 6 for β_1 and β_2 , in §7 we investigate how the inclusion of surfactant affects the velocity of an isolated bubble in a Hele-Shaw cell. Finally, in §8 we summarise our key findings.

2. Governing Equations

2.1. Dimensional modelling

We consider the steady propagation of a two-dimensional bubble inside a channel of height $2\hat{H}$ (see figure 1). We orient the \hat{x} -axis and the \hat{z} -axis along and perpendicular to the lower wall, respectively. We define i and k as the unit vectors in the \hat{x} - and \hat{z} -directions, respectively. We assume that buoyancy effects are negligible, so the flow is symmetric across the centreline of the channel and we can restrict our attention to the region $0 \leqslant \hat{z} \leqslant \hat{H}$. We define the bubble surface in this region to be at $\hat{z} = \hat{h}(\hat{x})$. The normal to the liquid surface pointing into the bubble and the tangent to the bubble surface are denoted by n, and t, respectively and are

116

117

118

119

126

140

112 given by

113
$$n = \frac{-\hat{h}_{\hat{x}}i + k}{\sqrt{1 + \hat{h}_{\hat{x}}^2}}, \qquad t = \frac{i + \hat{h}_{\hat{x}}k}{\sqrt{1 + \hat{h}_{\hat{x}}^2}}, \qquad (2.1)$$

where the subscript variable means partial differentiation with respect to that variable.

We assume the motion of the bubble is sufficiently slow that the flow is in the Stokes regime and we move into a frame of reference in which the bubble is stationary and the walls travel at a velocity $-\hat{U}_b i$, where \hat{U}_b is the bubble propagation speed. We denote the liquid velocity as $\hat{u} = (\hat{u}, \hat{v})$ and the pressure as \hat{p} . The motion of the liquid is then governed by the Stokes equations

120
$$\hat{\nabla} \cdot \hat{\boldsymbol{u}} = 0, \qquad \text{in } \hat{\Omega}, \qquad (2.2a)$$

121
$$\hat{\nabla}\hat{p} = \hat{\mu}\hat{\nabla}^2\hat{u} \qquad \text{in } \hat{\Omega}, \qquad (2.2b)$$

where $\hat{\mu}$ is the constant liquid viscosity, $\hat{\Omega}$ denotes the liquid region, and $\hat{\nabla} = (\partial/\partial\hat{x}, \partial/\partial\hat{z})$ is the two-dimensional gradient operator.

The surfactant concentration on the surface of the bubble, $\hat{\Gamma}$, is governed by the advection–diffusion–reaction equation (Stone 1990)

$$\frac{\mathrm{d}}{\mathrm{d}\hat{s}}\left(\hat{\Gamma}u_{S}\right) = \hat{D}\frac{\mathrm{d}^{2}\hat{\Gamma}}{\mathrm{d}\hat{s}^{2}} + \hat{k}_{1}\hat{C} - \hat{k}_{2}\hat{\Gamma}, \qquad \text{on} \quad \hat{z} = \hat{h}(\hat{x}), \tag{2.3}$$

where \hat{s} is arclength, \hat{D} is the surface diffusion coefficient, \hat{C} is the bulk concentration and

$$u_S = \hat{\boldsymbol{u}} \cdot \boldsymbol{t} \Big|_{\hat{z} = \hat{h}} \tag{2.4}$$

is the tangential surface velocity. We have supplemented (2.3) with a linear reaction term, 129 with rate constants \hat{k}_1 and \hat{k}_2 , because the surfactant concentration in the bulk and on 130 the surface are assumed to be close to equilibrium. There are numerous numerical studies 131 that include nonlinear reaction kinetics, such as Fujioka & Grotberg (2005) and Muradoglu 132 et al. (2019). In general one would solve a coupled advection—diffusion equation for \hat{C} but, as 133 mentioned above we focus on the "bulk equilibrium" limit in which the bulk concentration 134 does not vary significantly, so we take \hat{C} to be a known constant. We further assume that the 135 surfactant quickly adsorbs or desorbs onto the surface of the bubble and thus the surfactant 136 concentration is close to equilibrium. This implies that surfactant cannot accumulate and thus 137 the bubble cannot rigidify, a phenomenon seen in surfactant systems without fast reactions 138 (see e.g. Park 1992). 139

On the Hele-Shaw cell wall, we supply the no-slip boundary condition

$$\hat{\boldsymbol{u}} = -\hat{U}_b \boldsymbol{i} \qquad \qquad \text{on} \quad \hat{z} = 0. \tag{2.5a}$$

On the bubble surface, we supply a kinematic condition and normal and tangential stress balances:

144
$$\hat{\boldsymbol{u}} \cdot \boldsymbol{n} = 0 \qquad \text{on } \hat{z} = \hat{h}(\hat{x}), \qquad (2.5b)$$

145
$$\mathbf{n} \cdot \hat{\mathbf{\sigma}} \cdot \mathbf{n} = -\hat{p}_b + \hat{\gamma}\hat{\kappa}$$
 on $\hat{z} = \hat{h}(\hat{x}),$ (2.5c)

$$t \cdot \hat{\boldsymbol{\sigma}} \cdot \boldsymbol{n} = \frac{\mathrm{d}\hat{\boldsymbol{\gamma}}}{\mathrm{d}\hat{\boldsymbol{s}}} \qquad \text{on} \quad \hat{\boldsymbol{z}} = \hat{\boldsymbol{h}}(\hat{\boldsymbol{x}}), \tag{2.5d}$$

where $\hat{\gamma}$ is the (no longer constant) surface tension, $\hat{\kappa}$ is the curvature, \hat{p}_b is the constant

pressure inside the bubble, and $\hat{\sigma}$ is the viscous stress tensor, given by

$$\hat{\boldsymbol{\sigma}} = -\hat{p}\boldsymbol{I} + \hat{\mu}\left(\hat{\boldsymbol{\nabla}}\hat{\boldsymbol{u}} + \hat{\boldsymbol{\nabla}}\hat{\boldsymbol{u}}^{\mathrm{T}}\right),$$

- where I denotes the two-dimensional identity tensor and the superscript T denotes the transpose.
- We close our model with an equation of state, which relates the surface tension, $\hat{\gamma}$, to the
- surfactant surface concentration, $\hat{\Gamma}$. Since we are assuming that the surfactant concentrations
- in the bulk and on the surface are close to equilibrium, we also supply a linear equation of
- 155 state, i.e.,

$$\hat{\gamma} = \hat{\gamma}_0 + \frac{\mathrm{d}\hat{\gamma}}{\mathrm{d}\hat{\Gamma}}\Big|_{\hat{\Gamma} = \hat{\Gamma}_0} (\hat{\Gamma} - \hat{\Gamma}_0), \tag{2.6}$$

where $\hat{\Gamma}_0 = \hat{k}_1 \hat{C} / \hat{k}_2$ is the equilibrium concentration of surfactant and $\hat{\gamma}_0$ is the surface tension at equilibrium.

We non-dimensionalise the system (2.2)–(2.6) as follows (in which dimensionless variables are denoted without hats)

162
$$(\hat{x}, \hat{z}, \hat{s}, \hat{h}(\hat{x})) = \hat{H}(x, z, s, h(x)), \qquad \hat{\boldsymbol{u}} = \hat{U}_b \boldsymbol{u}, \qquad \hat{\gamma} = \hat{\gamma}_0 \gamma,$$
163
$$(\hat{p}, \hat{p}_b) = \frac{\hat{\gamma}_0}{\hat{H}}(p, p_b), \qquad \hat{\kappa} = \frac{\kappa}{\hat{H}}, \qquad \hat{\Gamma} = \hat{\Gamma}_0 \Gamma.$$
(2.7)

164 The dimensionless governing equations are given by

165
$$\nabla \cdot \boldsymbol{u} = 0, \qquad \nabla p = \text{Ca} \nabla^2 \boldsymbol{u} \qquad \text{in } 0 < z < h(x). \tag{2.8}$$

The dimensionless versions of the boundary conditions (2.5) are given by

$$\mathbf{u} = -\mathbf{i} \qquad \text{on} \quad z = 0, \tag{2.9a}$$

and, on the bubble surface z = h(x),

$$\frac{\mathrm{d}}{\mathrm{d}s} \left(\Gamma u_S \right) = \frac{1}{\mathrm{Pe}} \frac{\mathrm{d}^2 \Gamma}{\mathrm{d}s^2} + k(1 - \Gamma), \tag{2.9b}$$

$$v = uh_x, (2.9c)$$

171
$$p_b - p - \frac{2\text{Ca}}{1 + h_x^2} \left(\left(1 - h_x^2 \right) u_x + h_x (u_z + v_x) \right) = \frac{(1 - \text{Ma}(\Gamma - 1)) h_{xx}}{\left(1 + h_x^2 \right)^{3/2}}, \tag{2.9d}$$

172
$$\frac{1}{\left(1+h_x^2\right)^{1/2}} \left(-4h_x u_x + \left(1-h_x^2\right) (u_z + v_x)\right) = -\frac{\text{Ma}}{\text{Ca}} \Gamma_x, \tag{2.9e}$$

173 where

174
$$\frac{\mathrm{d}}{\mathrm{d}s} = \frac{1}{\sqrt{1 + h_x^2}} \frac{\mathrm{d}}{\mathrm{d}x} \qquad \text{and} \qquad u_S = \frac{u + h_x v}{\sqrt{1 + h_x^2}} \bigg|_{z = h(x)}.$$

The model (2.8)–(2.9) contains the dimensionless parameters

176
$$\operatorname{Ca} = \frac{\hat{\mu}\hat{U}_b}{\hat{\gamma}_0}, \qquad \operatorname{Pe} = \frac{\hat{H}\hat{U}_b}{\hat{D}}, \qquad \operatorname{Ma} = -\frac{\hat{\Gamma}_0}{\hat{\gamma}_0} \frac{\mathrm{d}\hat{\gamma}}{\mathrm{d}\hat{\Gamma}}, \qquad k = \frac{\hat{k}_2\hat{H}}{\hat{U}_b}, \tag{2.10}$$

namely the capillary number, the Péclet number, the Marangoni number and the dimension-177 less reaction constant, respectively. We consider slow flow in which $Ca \ll 1$. Furthermore, 178 we assume that Pe $\gg 1$, and hence we take the limit Pe $\to \infty$, so (2.9b) reduces to an 179 advection–reaction equation for Γ . Finally, we also consider the regime where $k \gg 1$ so that 180 the surface and bulk surfactant are approximately in equilibrium. We observe from (2.9b) that 181 $\Gamma \to 1$ as $k \to \infty$ and therefore define $\tau = k \text{Ca}^{1/3}(\Gamma - 1)$. Here the scaling of τ with $\text{Ca}^{1/3}$ 182 is designed to achieve dominant balances in the transition region between the capillary-static 183 meniscus and the thin film on the channel wall (marked Region 3 in figure 2), as we will show 184 below. We then identify a distinguished limit in which, although the surface concentration 185 of surfactant is almost constant, the Marangoni stress at the free surface is retained in the 186 model at leading order. To this end, we define the dimensionless elasticity parameter 187

$$E = \frac{Ma}{Cak} = -\frac{\hat{\Gamma}_0}{\hat{\mu}\hat{H}\hat{k}_2} \frac{d\hat{\gamma}}{d\hat{\Gamma}},\tag{2.11}$$

and take E = O(1) while letting $k \to \infty$. The surfactant conservation equation (2.9*b*) and boundary conditions (2.9*d*)–(2.9*e*) thus reduce to

$$Ca^{1/3}\frac{du_S}{ds} = \tau (2.12a)$$

192
$$p_b - p - \frac{2Ca}{1 + h_x^2} \left(\left(1 - h_x^2 \right) u_x + h_x (u_z + v_x) \right) = \frac{(1 - ECa^{2/3}\tau) h_{xx}}{\left(1 + h_x^2 \right)^{3/2}}, \tag{2.12b}$$

$$\frac{\operatorname{Ca}^{1/3}}{\left(1+h_{x}^{2}\right)^{1/2}}\left(-4h_{x}u_{x}+\left(1-h_{x}^{2}\right)\left(u_{z}+v_{x}\right)\right)=-E\tau_{x},\tag{2.12c}$$

194 all on z = h(x).

195

196

197

198

199

200

201

202203

204

205

208

212213

2.3. Summary of assumptions

Here we summarise the assumptions that have been made in this section.

- The bulk surfactant concentration \hat{C} is sufficiently large that it does not vary significantly due to interaction with the surface, and we can treat it as effectively constant.
- The surfactant is highly soluble, so the surface and bulk surfactant concentrations are approximately in equilibrium, i.e., $k \gg 1$.
 - Surface diffusion of surfactant is negligible, so Pe $\ll 1$.

Following these assumptions, our model for a highly soluble surfactant is given by (2.8) with the boundary conditions (2.9a), (2.9c), and (2.12). In addition, we will assume shortly that the bubble propagates sufficiently slowly for the capillary number Ca to be small.

3. The front of the bubble

3.1. Regions and scalings

We consider the small-Ca limit and perform a perturbation expansion in powers of $Ca^{1/3}$, following the analysis presented by Park & Homsy (1984), for the similar problem of a

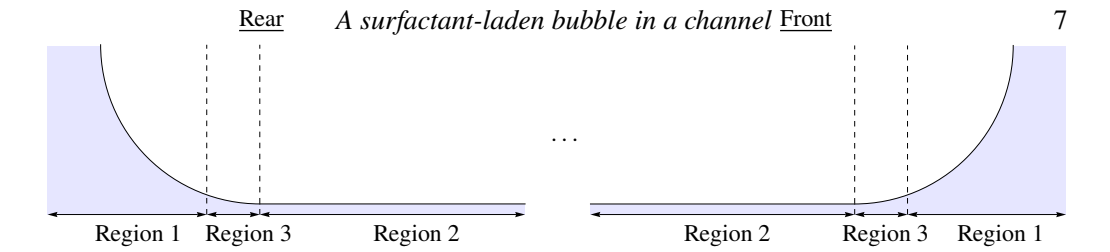


Figure 2: Schematic of the front and rear of a bubble, showing the three regions of interest in each: (1) front and rear cap regions, (2) thin film regions, (3) transition regions.

surfactant-free bubble. As shown by Park & Homsy, in the small-Ca limit the problem splits into three regions of interest (see figure 2).

216

217

227

- 1. The front-cap region. Here the free surface is capillary static and hence, to leading order, is a circular cap.
- 220 2. The thin film region. Through a lubrication analysis, we find there is a thin liquid film of constant thickness between the channel wall and the bubble.
- 3. The transition region. Here both viscous and capillary forces are important, which allows us to smoothly transition from the circular cap to the thin film region.
- We include for completeness the analysis of the front-cap and thin film regions, which follows directly from Park & Homsy. It is in the transition region where the effect of the surfactant is included, and thus the equations deviate from those found by Park & Homsy.

3.2. Region 1: Front-cap region

In this region we expand our variables in powers of $Ca^{1/3}$: $p(x, z) \sim p_0(x, z) + Ca^{1/3}p_1(x, z) + \cdots$ and so forth. At leading order, the equations of motion (2.8) become

$$\nabla \cdot \boldsymbol{u}_0 = 0, \qquad \nabla p_0 = \boldsymbol{0}, \qquad (3.1a,b)$$

while the boundary conditions (2.12*a*) and (2.12*c*) are both satisfied identically by $\tau_0 = 0$. Equation (3.1*b*) implies that $p_0 = \text{constant}$, and the normal stress balances at the bubble surface (2.12*b*) at leading order reads

234
$$\Delta p_0 = \frac{h_0''}{(1 + h_0'^2)^{3/2}} \qquad \text{on} \quad z = h_0(x), \tag{3.2}$$

where $\Delta p_0 = p_b - p_0$ is the leading-order difference between the constant pressure inside the bubble, p_b , and the fluid pressure.

To find the leading-order shape of the bubble, we impose the conditions $h_0(x) \to 1$ and $h_0'(x) \to \infty$ at the front tip of the bubble (which we define to be at x=0), and $h_0(x_c) = h_0'(x_c) = 0$, where $x_c < 0$ is the *a priori* unknown location of the point where the leading-order meniscus encounters the cell wall. We thus find that $\Delta p_0 = 1$ and $x_c = -1$, and the leading-order shape of the meniscus a circular cap of radius 1 (Park & Homsy 1984), given by

243
$$h_0(x) = 1 - \sqrt{1 - (x+1)^2},$$
 for $x \in (-1,0).$ (3.3)

In (1.2) we require knowledge of the pressure drop across the meniscus up to $O(Ca^{2/3})$. Following Park & Homsy (1984), we find that p_1 , $h_1 \equiv 0$; then at $O(Ca^{2/3})$ we find that p_2

is a constant, denoted by $-\beta_1$, and

$$\beta_1 = \frac{h_2^{"}}{(1 + h_0^{'2})^{3/2}},\tag{3.4}$$

248 which can be solved to give

$$h_2(x) = \beta_1 \sqrt{1 - (x+1)^2},\tag{3.5}$$

250 where β_1 is the *a priori* unknown $O(\text{Ca}^{2/3})$ pressure correction.

251 3.3. Region 2: Thin film region

252 In the thin film region, we rescale the variables as

253
$$x = \tilde{x},$$
 $z = Ca^{2/3}\tilde{z},$ $h = Ca^{2/3}\tilde{h},$ $p - p_b = Ca^{2/3}\tilde{p},$
254 $u = \tilde{u},$ $v = Ca^{2/3}\tilde{v}$ $\tau = Ca^{1/3}\tilde{\tau}.$ (3.6)

Again we expand the variables in powers of $Ca^{1/3}$. At leading order, the equations of motion (2.8) become

257
$$\tilde{u}_{0\tilde{x}} + \tilde{v}_{0\tilde{z}} = 0, \qquad \tilde{u}_{0\tilde{z}\tilde{z}} = 0, \qquad \tilde{p}_{0\tilde{z}} = 0.$$
 (3.7*a-c*)

The kinematic boundary conditions (2.9a) and (2.9c) become

259
$$\tilde{u}_0 = -1, \quad \tilde{v}_0 = 0$$
 on $\tilde{z} = 0,$ (3.8a)

$$\tilde{v}_0 = \tilde{u}_0 \tilde{h}_{0\tilde{x}} \qquad \text{on} \quad \tilde{z} = \tilde{h}_0(\tilde{x}), \tag{3.8b}$$

and the remaining boundary conditions (2.12a)–(2.12c) reduce to

262
$$\tilde{\tau}_0 = -\tilde{u}_{0x}, \qquad \tilde{p}_0 = \tilde{h}_{0xx}, \qquad \tilde{u}_{0\tilde{z}} = 0 \qquad \text{on } \tilde{z} = \tilde{h}_0(\tilde{x}).$$
 (3.9*a-c*)

Hence we find that $\tilde{\tau}_0 \equiv 0$, $\tilde{u}_0 \equiv -1$, $\tilde{p}_0 \equiv 0$ and $\tilde{h}_0(\tilde{x}) = \text{constant}$. Thus, region 2 has a constant (*a priori* unknown) film thickness

$$\tilde{h}_0 = \frac{\hat{h}_{\infty}}{\hat{H}Ca^{2/3}},\tag{3.10}$$

where \hat{h}_{∞} is the dimensional film thickness indicated in figure 1.

Next, we examine the transition region, which allows us to smoothly transition from the constant film region to the circular cap at the front of the bubble.

3.4. Region 3: Transition region

270 In the transition region, we shift the origin to x = -1 and rescale the variables as

$$x + 1 = \operatorname{Ca}^{1/3} X, \quad z = \operatorname{Ca}^{2/3} Z, \quad h = \operatorname{Ca}^{2/3} H, \quad p = P,$$

$$u = U, \qquad v = \operatorname{Ca}^{1/3} V, \quad \tau = G.$$
(3.11)

We again expand the variables in powers of $Ca^{1/3}$.

The leading-order equations of motion (2.8) become

274
$$U_{0X} + V_{0Z} = 0$$
, $P_{0X} = U_{0ZZ}$, $P_{0Z} = 0$ in $0 < Z < H_0(X)$. (3.12*a*-*c*)

The boundary conditions (2.9a) and (2.9c) become

$$U_0 = -1, \quad V_0 = 0$$
 on $Z = 0,$ (3.13a)

$$V_0 = U_0 H_{0X}$$
 on $Z = H_0(X)$, (3.13b)

278 and the remaining boundary conditions (2.12) become

279
$$G_0 = -U'_{S0}$$
, $-P_0 = H''_0$, $U_{0Z} = -EG'_0$ on $Z = H_0(X)$, (3.14*a*–*c*)

280 where $U_{S0}(X) = U_0(X, H_0(X))$.

Using (3.12)–(3.14), we find that U_0 is given by

$$U_0(X,Z) = -1 + \frac{1}{2}H_0^{\prime\prime\prime}(X)(2H_0(X)Z - Z^2) - EG_0^{\prime}(X)Z. \tag{3.15}$$

By integrating (3.15) across the liquid layer (from Z = 0 to $Z = H_0(X)$) we find that the flux of liquid in the *X*-direction is given by

$$Q = \frac{1}{3}H_0^{\prime\prime\prime}H_0^3 - \frac{1}{2}EG_0^{\prime}H_0^2 - H_0.$$
 (3.16)

286 By conservation of mass this quantity must equal the flux of liquid in the thin film region,

where $Q = -\tilde{h}_0$. We thus obtain an equation for the height of the bubble surface in the

288 transition region, namely

301

$$H_0^{\prime\prime\prime} = \frac{3(H_0 - \tilde{h}_0)}{H_0^3} + \frac{3EG_0^{\prime}}{2H_0}.$$
 (3.17)

Next, using (3.15) and (3.17), we find that (3.14a) becomes

$$\frac{\mathrm{d}}{\mathrm{d}X} \left(\frac{1}{4} E G_0' H_0 + \frac{3\tilde{h}_0}{2H_0} \right) = G_0. \tag{3.18}$$

Equations (3.17) and (3.18) form a closed system for the film profile, $H_0(X)$, and the perturbation to the surface concentration of surfactant, $G_0(X)$ in the transition region. In

294 addition, we enforce the matching conditions

295
$$H_0(X) \to \tilde{h}_0$$
, $G_0(X) \to 0$ as $X \to -\infty$, (3.19a)

296
$$H_0(X) \sim \frac{1}{2}X^2 + \beta_1, \qquad G_0(X) \to 0 \quad \text{as} \quad X \to \infty.$$
 (3.19b)

In principle, the solution of the system (3.17)–(3.18) subject to the far-field behaviour (3.19)

determines the *a priori* unknown constants \tilde{h}_0 and β_1 along with H_0 and G_0 .

In the next section, we analyse the problem (3.17)–(3.19).

4. Analysis of the transition region equations

4.1. Normalisation

We begin by normalising the equations (3.17) and (3.18) by scaling the variables as

303
$$\xi = \frac{X + S}{\tilde{h}_0}, \qquad \eta(\xi) = \frac{H_0(X)}{\tilde{h}_0}, \qquad g(\xi) = \tilde{h}_0 G_0(X).$$
 (4.1)

The equations (3.17) and (3.18) are translation invariant, so we introduce an arbitrary shift S to simplify the forthcoming analysis. Under these scalings, (3.17) and (3.18) become

$$\eta''' = \frac{3(\eta - 1)}{\eta^3} + \frac{3\mathcal{E}g'}{2\eta},\tag{4.2a}$$

$$\frac{\mathcal{E}}{4} \left(\eta g' \right)' = g + \frac{3\eta'}{2\eta^2},\tag{4.2b}$$

308 where

$$\mathcal{E} = \frac{E}{\tilde{h}_0}.\tag{4.3}$$

The boundary conditions (3.19) imply that

311
$$\eta(\xi) \to 1$$
, $g(\xi) \to 0$ as $\xi \to -\infty$, (4.4a)

$$g(\xi) \to 0$$
 as $\xi \to \infty$. (4.4b)

The solution of (4.2a) can be shown to behave quadratically as $\xi \to \infty$ so

314
$$\eta(\xi) \sim \frac{1}{2}a\xi^2 + b\xi + c \qquad \text{as} \quad \xi \to \infty, \tag{4.5}$$

- where a, b and c are constants. Notice that the coefficients are not uniquely determined due to
- the arbitrary choice of origin for ξ . However, the translation-invariant groups a and $ac \frac{1}{2}b^2$
- are uniquely determined. By comparison with (3.19), we see that they are related to the a
- 318 *priori* unknown constants \tilde{h}_0 and β_1 by

319
$$a = \tilde{h}_0, \qquad ac - \frac{1}{2}b^2 = \beta_1. \tag{4.6}$$

- The solution strategy for the problem (4.2)–(4.4) is explained in the following subsection.
- Once η and g have been computed for a given value of E, the surface velocity of the thin film
- 322 is calculated from (3.15), giving

$$U_S = \frac{1}{2} - \frac{\mathcal{E}}{4} \eta g' - \frac{3}{2\eta}. \tag{4.7}$$

We solve (4.2) numerically by shooting from $\xi \to -\infty$. Linearising (4.2) about the far-field behaviour (4.4a), we find that

327
$$\eta(\xi) \sim 1 + \sum_{n=1}^{5} A_n e^{\lambda_n \xi}, \qquad g(\xi) \sim \sum_{n=1}^{5} B_n e^{\lambda_n \xi} \qquad \text{as} \quad \xi \to -\infty, \tag{4.8}$$

where the λ_n are roots of the quintic polynomial

$$\lambda^5 - \frac{4}{\varepsilon}\lambda^3 - 12\lambda^2 + \frac{12}{\varepsilon} = 0. \tag{4.9}$$

- This equation has two real and positive roots (which we label λ_1 and λ_2), one real and negative
- (labelled λ_3), and a complex conjugate pair with negative real part (labelled λ_c and $\bar{\lambda}_c$). We
- require the solution to decay as $\xi \to -\infty$, so only the positive eigenvalues are permitted.
- 333 Hence the decaying linearised far-field behaviour is given by

334
$$\eta(\xi) \sim 1 + A_1 e^{\lambda_1 \xi} + A_2 e^{\lambda_2 \xi}$$
 as $\xi \to -\infty$, (4.10a)

335
$$g(\xi) \sim \frac{\lambda_1 \left(\lambda_1^3 - 12\right) A_1}{6} e^{\lambda_1 \xi} + \frac{\lambda_2 \left(\lambda_2^3 - 12\right) A_2}{6} e^{\lambda_2 \xi} \quad \text{as} \quad \xi \to -\infty,$$
 (4.10b)

- where A_1 and A_2 are a priori unknown constants. Due to the translation invariance we may
- 337 (e.g.) set $A_1 = \pm 1$ by choice of S in (4.1). We then determine A_2 via the shooting method
- 338 to ensure our solution satisfies $g(\xi) \to 0$ as $\xi \to \infty$.

[†] Although translation allows us to set the coefficient of one exponential to have magnitude 1, we do not know its sign in advance; however, we always find that in the front transition region $A_1 > 0$.

For each value of \mathcal{E} , we use the above shooting method to solve for η and g, then read off the coefficients $\{a, b, c\}$ in the quadratic behaviour (4.5) as $\xi \to \infty$. We then use (4.3) and (4.6) to determine $a = \tilde{h}_0$ and β_1 parametrically as functions of E. However, the shooting problem can become delicate for small or large values of \mathcal{E} . In the next two subsections, we present asymptotic results for these two limits.

344 4.3. *Small-E limit*

In the limit where \mathcal{E} is small we expand

346
$$\eta \sim \eta_0 + \mathcal{E}\eta_1 + \cdots, \qquad g \sim g_0 + \mathcal{E}g_1 + \cdots.$$
 (4.11)

This regime is similar to that studied by Waters & Grotberg (2002) for a surfactant-laden liquid plug and by Ginley & Radke (1989) who considered a bubble in a capillary tube.

At O(1) in (4.2), we find that

349

$$\eta_0^{\prime\prime\prime} = \frac{3(\eta_0 - 1)}{\eta_0^3},\tag{4.12a}$$

$$g_0 = -\frac{3\eta_0'}{2\eta_0^2}. (4.12b)$$

The decoupled equation (4.12a) for η_0 is the same Landau–Levich equation used by 352 Bretherton (1961) to determine the shape of a surfactant-free bubble in the transition 353 region. The solution for η_0 is uniquely determined, up to an arbitrary translation, and 354 355 the corresponding leading-order surfactant concentration profile $g_0(\xi)$, given by (4.12b), is plotted in figure 3. Although the limit $\mathcal{E} \to 0$ is singular, removing the highest derivative 356 in (4.2b), we see that g_0 tends to zero in the far field, as required, and no boundary-layer 357 behaviour is produced, as also found by Waters & Grotberg (2002) and Ginley & Radke 358 359 (1989). The coefficients in the quadratic behaviour

360
$$\eta_0(\xi) \sim \frac{1}{2}a_0\xi^2 + b_0\xi + c_0$$
 as $\xi \to \infty$, (4.13a)

are also determined uniquely and, in particular, we have $a_0 \approx 1.337$ and $a_0c_0 - \frac{1}{2}b_0^2 \approx 3.88$, as found by Bretherton (1961).

To find the correction to \tilde{h}_0 and β_1 due to the effect of surfactants, we proceed to first order in (4.2a) to obtain the equation

$$\eta_1^{\prime\prime\prime} = \frac{12(3 - 2\eta_0)\eta_1 + 9(2\eta_0^{\prime 2} - \eta_0\eta_0^{\prime\prime})}{4\eta_0^4},\tag{4.14}$$

for the correction to the thin film height. We solve (4.14) in the same fashion as (4.12*a*) by shooting from $\xi \to -\infty$. Again the solution to (4.14) behaves quadratically for large positive ξ :

369
$$\eta_{01} \sim \frac{1}{2} a_1 \xi^2 + b_1 \xi + c_1$$
 as $\xi \to \infty$, (4.15a)

where the constants a_1 , b_1 , c_1 are in principle determined (up to an arbitrary translation) by the solution of (4.14). In particular we find that $a_1 \approx -0.0146$, and $a_0c_1+c_0a_1-b_0b_1 \approx 0.58$. Finally, we obtain the small-E expansions for $a = \tilde{h}_0$ and β_1 from (4.6). Note that the definition (4.3) of \mathcal{E} involves \tilde{h}_0 , so we have to manipulate the expansions to remove the

374 dependence on \tilde{h}_0 to get

375
$$a \sim a_0 + \frac{a_1}{a_0} E \approx 1.337 - 0.011E$$
 as $E \to 0$, (4.16a)

$$\beta_1 \sim a_0 c_0 - \frac{1}{2} b_0^2 + \frac{a_0 c_1 + c_0 a_1 - b_0 b_1}{a_0} E \approx 3.88 + 0.43E \quad \text{as} \quad E \to 0.$$
 (4.16b)

We note that (4.16a) and (4.16b) differ from (26) in Waters & Grotberg (2002) because they include a factor of 3 in their Ca, which induces a factor of $3^{1/3}$ in the definition of E. We also note that Waters & Grotberg's expression for the pressure drop is twice ours, due to the

380 cylindrical instead of two-dimensional geometry that they study.

In the other extreme where \mathcal{E} is large, we expand

$$\eta \sim \eta_0 + \frac{1}{\mathcal{E}} \eta_1 + \cdots, \qquad g \sim \frac{1}{\mathcal{E}} g_1 + \cdots. \tag{4.17}$$

384 At O(1) in (4.2) we find

391

392

393

394

395

$$\eta_0^{\prime\prime\prime} = \frac{3(\eta_0 - 1)}{\eta_0^3} + \frac{3g_1^{\prime}}{2\eta_0},\tag{4.18a}$$

$$\frac{1}{4}(g_1'\eta_0)' = \frac{3\eta_0'}{2\eta_0^2}. (4.18b)$$

We can integrate (4.18b) and substitute into (4.18a) to obtain

$$\eta_0^{\prime\prime\prime} = \frac{12(\eta_0 - 1)}{\eta_0^3},\tag{4.19a}$$

$$g_1 = \frac{1}{2} \eta_0 \eta_0^{"} - \frac{1}{4} (\eta_0^{\'})^2 - \frac{1}{2} \beta_{10}, \tag{4.19b}$$

where β_{10} is the leading-order approximation for the coefficient β_1 .

Once again, (4.19a) is the Landau–Levich equation and it is similar to the surfactant-free equation (4.12a) found by Bretherton (1961) except with an additional factor of 4 in the numerator. This additional factor of 4 induces an increase in the thin film height and correction to the pressure drop by a factor of $4^{2/3}$, i.e.,

$$a \to 4^{2/3} \cdot 1.337 \approx 3.369$$
 as $E \to \infty$, (4.20a)

396
$$\beta_1 \to \beta_{10} \approx 4^{2/3} \cdot 3.88 \approx 9.78$$
 as $E \to \infty$. (4.20b)

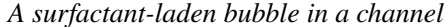
In this limit, we find that the surface velocity (4.7) is given by $U_S \equiv -1$, which corresponds to the bubble interface travelling at the same velocity as the walls of the cell.

These results reproduce the large-Marangoni-number limit reported in previous studies (see, for example, Ratulowski & Chang 1990; Park 1992; Stebe & Barthes-Biesel 1995; Shen et al. 2002). However, we also evaluate the correction to the surfactant concentration, given by (4.19b) and plotted in figure 5, where it is evident that g_1 does not satisfy the far-field condition $g_1(\xi) \to 0$ as $\xi \to -\infty$. This apparent inconsistency can be resolved by examining an outer region in which

405
$$\xi = \mathcal{E}^{1/2}\Xi$$
, $g(\xi) = \mathcal{E}^{-1}\Psi(\Xi)$, $\eta(\xi) \sim 1 + \text{exponentially small terms}$, (4.21)

406 so that (4.2b) is transformed to

$$\Psi^{\prime\prime} = 4\Psi, \tag{4.22}$$



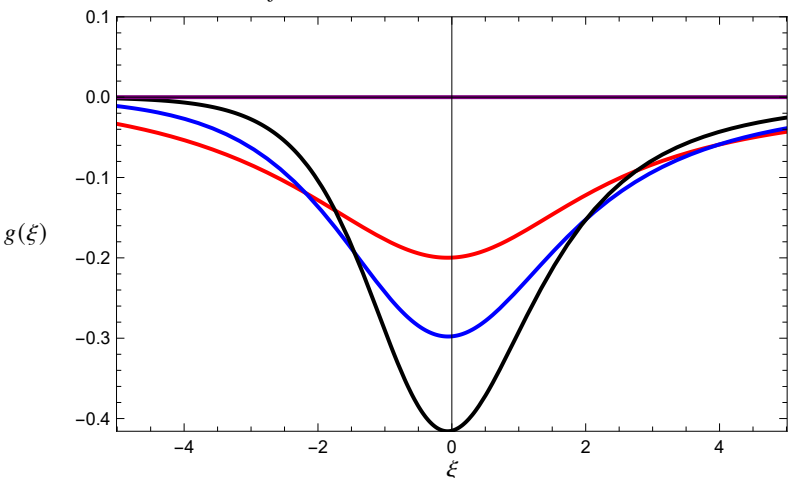


Figure 3: The surfactant concentration in the front transition region, $g(\xi)$, with $\mathcal{E} \to 0$ (black), $\mathcal{E} = 1$ (blue), $\mathcal{E} = 4$ (red), and $\mathcal{E} \to \infty$ (purple).

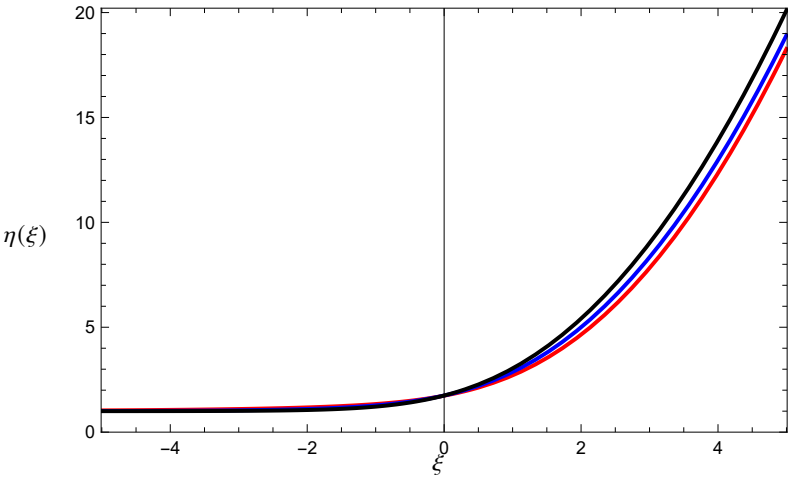


Figure 4: The free surface profile $\eta(\xi)$ in the front transition region, with $\mathcal{E} \to 0$ (black), $\mathcal{E} = 1$ (blue), $\mathcal{E} = 4$ (red)

up to exponentially small corrections. By matching with (4.19b) we thus obtain the leading-order outer solution

$$\Psi_0(\Xi) = -\frac{1}{2}\beta_{10}e^{2\Xi}.$$
 (4.23)

4.5. *Results*

408

409

In figure 3, we plot the correction from equilibrium to the surfactant concentration, g, in the 412 front transition region when $\mathcal{E} \to 0$, $\mathcal{E} = 1$, $\mathcal{E} = 4$ and $\mathcal{E} \to \infty$. We use the arbitrary shift 413 S introduced in §4.1 to align the peaks of the concentration profiles. In the limit $\mathcal{E} \to \infty$, 414 g vanishes across the entire domain, but in all other cases, we observe that g < 0 and so 415 the surfactant concentration is everywhere below equilibrium in the front transition region. 416 Similar concentration profiles were observed by Stebe & Barthes-Biesel (1995) in a system 417 with an elevated bulk concentration. In figure 4 we plot the film height in the transition region 418 419 and, for all values of \mathcal{E} , we observe similar profiles to those found by Bretherton (1961) and Park & Homsy (1984) for a surfactant-free bubble. 420

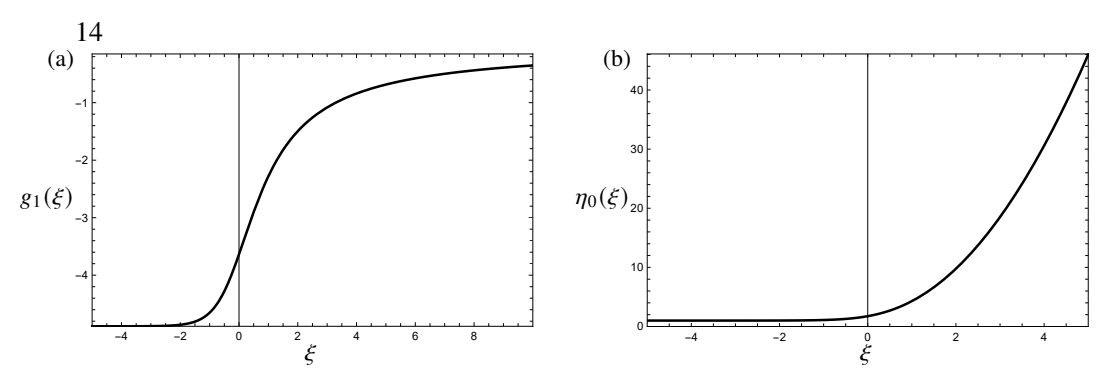


Figure 5: The leading-order (a) perturbation to the surfactant concentration, $g_1(\xi)$, and (b) free surface profile, $\eta_0(\xi)$, in the front transition region in the limit $\mathcal{E} \to \infty$.

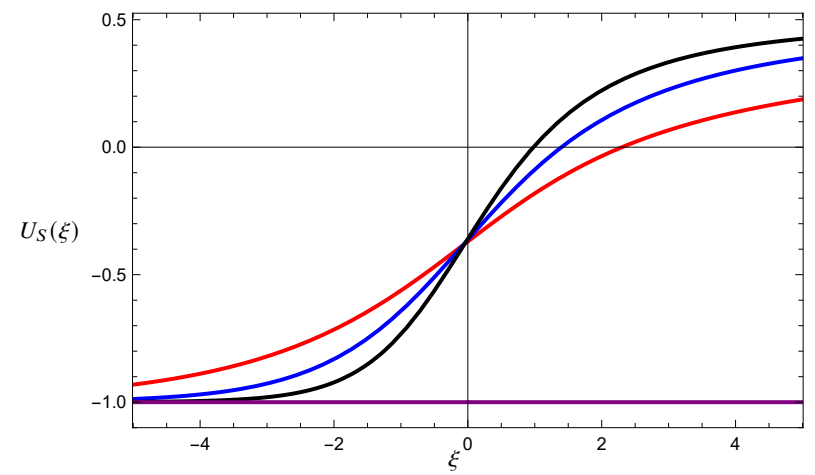


Figure 6: The surface velocity, $U_S(\xi)$, in the front transition region with $\mathcal{E} \to 0$ (black), $\mathcal{E} = 1$ (blue), $\mathcal{E} = 4$ (red), and $\mathcal{E} \to \infty$ (purple).

We plot the lowest-order perturbation to the surfactant concentration, $g_1(\xi)$, and the film height, $\eta_0(\xi)$, in the limit $\mathcal{E} \to \infty$ in figure 5. The leading-order solution evidently does not satisfy the downstream boundary condition $g_1(\xi) \to 0$ as $\xi \to -\infty$, implying that there must be a boundary layer at infinity, as explained in §4.4. In figure 6 we plot the leading-order surface velocity, U_S , for $\mathcal{E} \to 0$, $\mathcal{E} = 1$, $\mathcal{E} = 4$ and $\mathcal{E} \to \infty$. We observe that, for finite \mathcal{E} , there is a stagnation point (in the frame of the bubble) within the transition region. Its location is close to the minimum point of g in figure 3, because the flow directed outwards advects surfactant away from the stagnation point. The presence of a stagnation point along the front of the bubble is a prevalent feature of gas bubbles in Hele-Shaw cells or capillary tubes, even in systems with more complicated surfactant dynamics and non-zero Reynolds numbers (Fujioka & Grotberg 2005; Zheng et al. 2007).

The normalised height of the thin film, a, is plotted as a function of the elasticity parameter E in figure 7. As $E \to 0$, surfactant effects become negligible and the thin film height approaches Bretherton's result of 1.337 for a surfactant-free bubble (Bretherton 1961). At the other extreme, when E is large, a approaches 3.369 which is larger by a factor of $4^{2/3}$, as expected. Interestingly, (4.16a) predicts a decrease in the thin film height for small E (see figure 7(b)), however, figure 7(b) shows that the asymptotic result (4.16a) (also obtained by Waters & Grotberg 2002) quickly becomes redundant, and the normalised thin film height, a, increases with E thereafter.

The correction to the pressure drop across the front meniscus, β_1 , is plotted as a function of

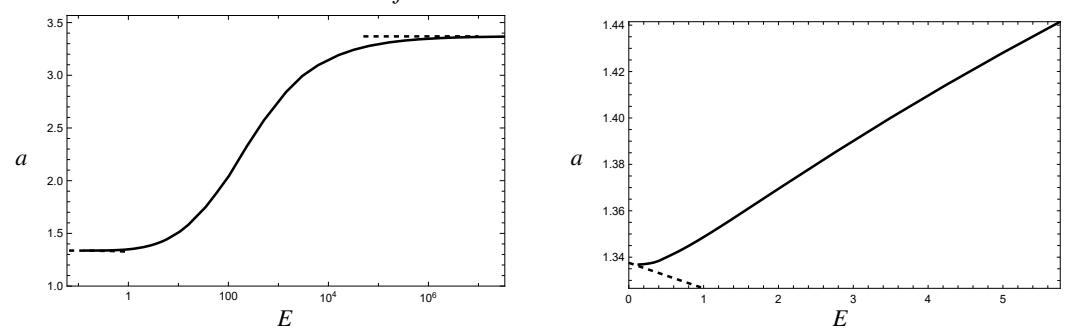


Figure 7: The normalised thin film height a versus elasticity parameter E. The solid curve is from the numerical solution of (4.2), and dashed curves are the asymptotic predictions: (4.16a) for small E and (4.20a) for large E. (a) A log-linear plot to show the full range of E. (b) The solution for $0 \le E \le 5.77$.

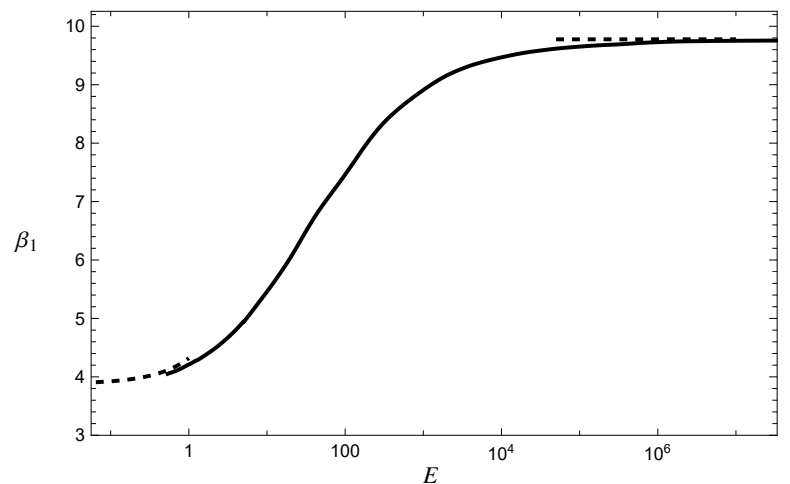


Figure 8: The correction to the pressure drop across the front meniscus, β_1 , versus elasticity parameter E. The solid curve is from the numerical solution of (4.2), and dashed curves are the asymptotic predictions: (4.16b) for small E and (4.20b) for large E.

E in figure 8. Again when E is small we recover the Bretherton (1961) result that $\beta_1 \approx 3.88$. We observe that β_1 is a monotonic increasing function and when E is large β_1 approaches 9.78, in agreement with (4.20b). In the numerical simulation of (4.2), accurate convergence for the value of β_1 could not be achieved for values of $E \leq 0.5$ due to the sensitivity of the numerical shooting method, caused by the singular nature of the system (4.2) as $E \to 0$. In general, it is harder to compute the value of β_1 than a at small E because a significantly larger value of ξ is needed to robustly extract the value of $ac - b^2/2$ from the quadratic function (4.5) than to determine a. The numerical approach is thus useful provided $E \gtrsim O(1)$, while the asymptotic approximation (4.16b) is useful when E is small, and we are reassured by figure 8 that there is at least a small overlap region where they approximately agree.

5. Rear of the bubble

5.1. Regions

As for the front meniscus, in the small-Ca limit the problem at the rear of the bubble splits into three regions of interest (see figure 2). In particular, for the rear cap region, we can follow the

466

same analysis as in §3.2 and find that the leading-order shape and surfactant concentration 455 are given by 456

$$h_0(x) = 1 - \sqrt{1 - (l - 1 + x)^2}, \tag{5.1a}$$

458
$$h_2(x) = \beta_2 \sqrt{(x+l)(2-l-x)}, \tag{5.1b}$$

$$\Gamma_0(x) = 1, \tag{5.1c}$$

- where l is the dimensionless length of the bubble, and β_2 is the a priori unknown $O(\text{Ca}^{2/3})$ 460 correction to the pressure drop across the rear meniscus. 461
- As in §3.3, in the thin film region (region 2), the film height \tilde{h}_0 is constant, and now in 462 principle known from the solution for the front meniscus (see figure 7). In the next section 463 we analyse the equation in the rear transition region in a similar manner to §4. 464

6. Analysis of the rear transition region equations

6.1. Normalisation

We again normalise by scaling the variables as 467

468
$$\xi = \frac{X + S}{\tilde{h}_0}, \qquad \eta(\xi) = \frac{H_0(X)}{\tilde{h}_0}, \qquad g(\xi) = \tilde{h}_0 G_0(X), \qquad (6.1)$$

where S is an arbitrary shift of our coordinates. We obtain exactly the same equations (4.2) 469 as the front transition region, i.e., 470

$$\eta''' = \frac{3(\eta - 1)}{\eta^3} + \frac{3\mathcal{E}g'}{2\eta},\tag{6.2a}$$

472
$$\frac{\mathcal{E}}{4}(g'\eta)' = g + \frac{3\eta'}{2\eta^2}.$$
 (6.2b)

We solve (6.2) numerically now by shooting from $\xi \to \infty$. We find that the decaying 473 linearised solution is given by 474

475
$$\eta \sim 1 \pm e^{\lambda_3 \xi} + S e^{\lambda_R \xi} \cos(\lambda_I \xi - q), \tag{6.3a}$$

476
$$g \sim \pm \frac{6\lambda_3}{\mathcal{E}\lambda_3^2 - 4} e^{\lambda_3 \xi} - S\Lambda_c(\lambda_R, \lambda_I) e^{\lambda_R \xi} \cos(\lambda_I \xi - q) - S\Lambda_s(\lambda_R, \lambda_I) e^{\lambda_R \xi} \sin(\lambda_I \xi - q),$$
(6.3b)

- as $\xi \to \infty$. Here, S and q are a priori unknown shooting parameters, λ_3 is the real negative 477 solution of (4.9), and $\lambda_c = \lambda_R + i\lambda_I$ is the complex root with negative real part. The 478 coefficients are given by 479

480
$$\Lambda_{c}(\lambda_{R}, \lambda_{I}) = \frac{6\lambda_{R}(-4 + \mathcal{E}(\lambda_{R}^{2} + \lambda_{I}^{2}))}{16 + 8\mathcal{E}(\lambda_{I}^{2} - \lambda_{R}^{2}) + \mathcal{E}^{2}(\lambda_{R}^{2} + \lambda_{I}^{2})^{2}},$$
 (6.4a)

481
$$\Lambda_s(\lambda_R, \lambda_I) = \frac{6\lambda_I (4 + \mathcal{E}(\lambda_R^2 + \lambda_I^2))}{16 + 8\mathcal{E}(\lambda_I^2 - \lambda_R^2) + \mathcal{E}^2(\lambda_R^2 + \lambda_I^2)^2}.$$
 (6.4b)

- Note again that the \pm occurs in (6.3) because although translation allows us to set the 482
- coefficient of the exponential to be of magnitude 1, we do not know its sign in advance. 483
- Finally, we now have that η_0 behaves quadratically for large negative ξ , i.e., 484

485
$$\eta \sim \frac{1}{2}A\xi^2 + B\xi + C \qquad \text{as} \quad \xi \to -\infty. \tag{6.5}$$

We solve (6.2) for each value of $\mathcal{E} = E/\tilde{h}_0(E)$ by applying a shooting method with two 486 unknown parameters S and q, which are fixed by ensuring $g(\xi) \to 0$ and $\eta''(\xi) \to \tilde{h}_0(E)$ as 487 $\mathcal{E} \to -\infty$, where $\tilde{h}_0(E)$ is as shown in figure 7. The first condition corresponds to matching 488 the surfactant concentration in the thin film to the equilibrium concentration in the rear cap 489 (see §5.1), and the second ensures that the thin film height at the rear meniscus matches the 490 height of the thin film deposited at the front meniscus. Following the matching procedure 491 laid out in §4.1, we then obtain the $O(\text{Ca}^{2/3})$ correction to the pressure drop across the rear 492 meniscus as 493

$$\beta_2 = AC - \frac{1}{2}B^2. {(6.6)}$$

This two-parameter shooting problem can be extremely sensitive, so we examine the limiting cases using asymptotic analysis.

497 6.2. Small & limit

In the extreme where \mathcal{E} is small we expand

494

505

506

507

508 509

$$\eta \sim \eta_0 + \mathcal{E}\eta_1 + \cdots, \tag{6.7a}$$

$$g \sim g_0 + \mathcal{E}g_1 + \cdots \tag{6.7b}$$

Then at O(1) in (6.2) we again find that the equations reduce to (4.12). We note that (6.2b) is singular in the limit $\mathcal{E} \to 0$; however, for the same reasons as presented in §4.3 there is no boundary-layer behaviour and the solution of (4.12b) satisfies all the relevant boundary conditions.

Again, the equation (4.12a) for η_0 decouples and is just the usual Landau–Levich equation obtained for a surfactant-free bubble. At first order in (6.2) we again obtain equation (4.14) for the correction to the bubble surface. We solve (4.14) by shooting from $\xi \to \infty$. Following the matching methodology laid out in §4.1, we thus find that the $O(\operatorname{Ca}^{2/3})$ correction to the pressure drop is given by

$$\beta_2 \sim -1.13 - 0.73E$$
 as $E \to 0$. (6.9)

The leading term in (6.9) is Bretherton's classical result for the rear meniscus of a surfactantfree bubble (Bretherton 1961), and the second term is the first correction due to the presence of surfactant.

514 6.3. *Large E limit*

In this limit we follow the same methodology as in §4.4 to obtain

$$\eta_0^{\prime\prime\prime} = \frac{12(\eta_0 - 1)}{\eta_0^3}.\tag{6.10}$$

Matching with the rear cap solutions (5.1) we find that the correction to the pressure drop is then given by

519
$$\beta_2 \sim -4^{2/3} \cdot 1.13 \approx -2.85$$
 as $E \to \infty$. (6.11)

Again this is a factor of $4^{2/3}$ larger than the original Bretherton (1961) result. This extends the large Marangoni number limit reported in many studies (see, for example, Ratulowski &

522 Chang 1990; Park 1992) to the rear meniscus.

In figure 9 we show example solutions for E = 1.36 (E = 1) and E = 5.76 (E = 4). In figure 9(b) we observe that the surfactant concentration can be both above and below the

535

555

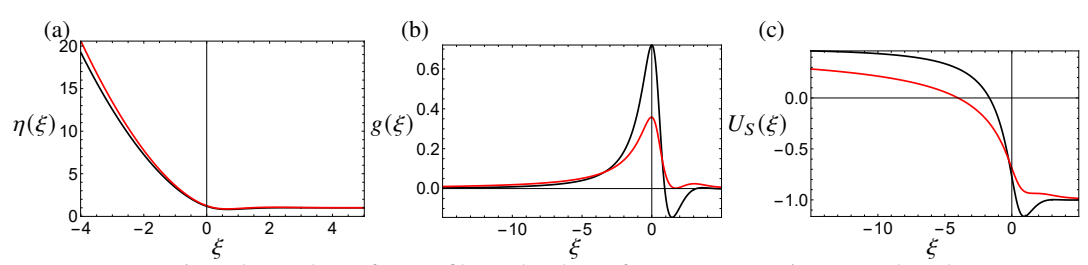


Figure 9: (a) The surface profile, η , (b) The surfactant concentration, g_1 , and (c) the surface velocity, U_S , in the rear transition region with $\mathcal{E} = 1$, (black) $\mathcal{E} = 4$ (red).

526 equilibrium concentration in the rear transition region, in contrast to the front transition region, where the concentration is always below equilibrium. For these specific solutions, we 527 find that $\beta_2 \approx -1.50$ for E=1 and $\beta_2 \approx -2.33$ for E=4, which are greater in magnitude 528 than the pressure drop $\beta_2 \approx -1.13$ for a surfactant-free bubble found by Bretherton (1961). 529 In figure 9(c) we plot the corresponding surface velocities, U_S for the same values of E. 530 Similarly to the front meniscus, we observe a stagnation point (in the frame of the bubble) in 531 the transition region. However, here the flow is directed into the stagnation point, resulting 532 in a local increase in the surfactant concentration. 533

7. Application to the motion of bubbles in a Hele-Shaw cell

7.1. Force balance

We are now in a position to include the effect of surfactants in the models presented by Booth et al. (2023, 2025a,b); Wu et al. (2024) for the motion of an approximately circular bubble in a Hele-Shaw cell moving due to a uniform background flow $\hat{U}_f i$. Booth et al. (2023) find that the dimensionless velocity U_b of such a bubble is determined by the force balance

$$\frac{\boldsymbol{U}_b}{|\boldsymbol{U}_b|^{1/3}} = \frac{\delta}{\pi} \oint_{\partial \Omega} -p\boldsymbol{n} \, \mathrm{d}s, \tag{7.1}$$

where $\partial\Omega$ is the bubble surface as viewed from above (see figure 10) and the *Bretherton* parameter is defined by

$$\delta = \frac{3\sqrt{\pi}\Gamma(11/6)}{(\beta_1 - \beta_2)\Gamma(4/3)} \frac{\text{Ca}_f^{1/3}}{\epsilon}.$$
 (7.2)

Here $\epsilon = \hat{H}/\hat{R}$, where \hat{R} is the radius of the bubble (measured from above), and $\text{Ca}_f = \hat{\mu}\hat{U}_f/\hat{\gamma}$ 544 is the capillary number based on the background flow speed, \hat{U}_f , both of which are assumed 545 to be small. In the distinguished limit where $Ca_f = O(\epsilon^3)$ as $\epsilon \to 0$, so the viscous 546 lubrication pressure balances the pressure drop across the menisci, the bubble is circular to 547 leading order (Booth et al. 2023). For a surfactant-free bubble, β_1 and β_2 are given by the 548 values $\beta_1(0) \approx 3.88$ and $\beta_2(0) \approx -1.13$ originally calculated by Bretherton. This result is 549 now easily generalised for a surfactant-laden bubble by using the expressions for $\beta_1(E)$ and 550 $\beta_2(E)$ found in §§4 and 6, respectively. Crucially, we recall that the elasticity parameter E, 551 given by (2.10), is independent of the capillary number, so the values of β_1 and β_2 depend 552 only on the given surfactant properties and concentration. Note that the values of β_1 and β_2 553 554 are both O(1) for the entire range of values of $E \in [0, \infty)$.

From (7.1), we find that the velocity of an isolated bubble in a uniform background flow

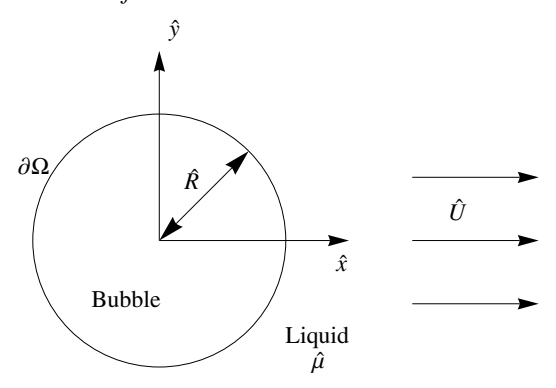


Figure 10: Plan view of a surfactant-laden bubble in a Hele-Shaw cell in a uniform background flow.

is given by $U_b = U_b i$, where

561

562

563

564

565

566567

568

569

570

571

572

573

574

575

576

577

578

$$\frac{U_b^{2/3}}{2 - U_b} = \delta = \left(\frac{\beta_1(0) - \beta_2(0)}{\beta_1(E) - \beta_2(E)}\right) \delta_B,\tag{7.3}$$

and we define the surfactant-free Bretherton parameter

$$\delta_B = \frac{3\sqrt{\pi}\Gamma(11/6)}{(\beta_1(0) - \beta_2(0))\Gamma(4/3)} \frac{\mathrm{Ca}_f^{1/3}}{\epsilon} \approx 1.12 \frac{\mathrm{Ca}_f^{1/3}}{\epsilon}.$$
 (7.4)

560 7.2. *Resul*

In figure 11 we plot U_b versus δ_B , for a range of values of E. Note that, if we plotted versus the Bretherton parameter, δ given by (7.2), then all the curves would collapse. Plotting U_b versus δ_B allows us to analyse the effect of surfactant on the bubble velocity in comparison with a surfactant-free bubble experiencing the same flow conditions. We observe that the velocity of a surfactant-laden bubble (E > 0) at each δ_B is less than that of a surfactant-free bubble (E = 0) at the same value of δ_B . This trend continues as we increase E, up to the limiting case $E \to \infty$ when $\delta = 4^{2/3}\delta_B$, the maximum value that δ can take for a fixed δ_B . Hence, we always find that a surfactant-laden bubble travels more slowly than a surfactant-free bubble under the same flow conditions.

The form of (7.3) has the same structure as the expression found by Baué *et al.* (2025) (their (5.11)) for the velocity of a droplet in a highly soluble surfactant solution, in the limit as the droplet viscosity tends to zero. Note that their capillary number is calculated from the droplet velocity, whereas we use the capillary number Ca_f based on the background flow speed. One can make an analogy between their constant 1/K and the prefactor of δ_B in (7.4). Our model provides the dependence of this prefactor on the surfactant properties, which is missing in their work. Baué *et al.* (2025) found experimentally that, with highly soluble surfactants, the velocity of a bubble increases with its size, which is consistent with (7.3).

8. Conclusions

In this paper, we develop a model for the propagation of a two-dimensional surfactant-laden bubble in a channel. We adopt the so-called bulk equilibrium model, in which there is assumed to be an abundance of surfactant in the liquid. We then identify a distinguished asymptotic limit in which the reaction kinetics are so fast that the surface concentration of surfactant remains close to equilibrium, but the Marangoni stress is large enough still to enter

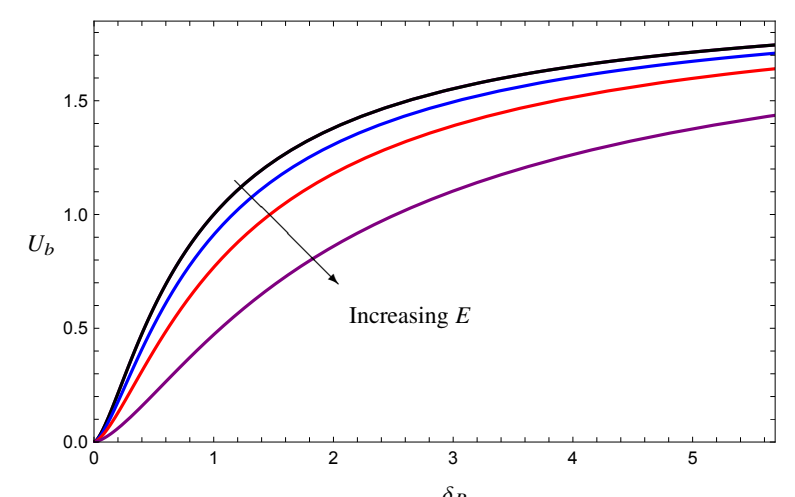


Figure 11: The dimensionless bubble velocity, U_b (7.3) as a function of the surfactant-free Bretherton parameter, δ_B (7.4) for a range of values of E=0 (black), E=1.36 (E=1) (blue), E=5.76 (E=4) (red), $E=\infty$ (purple), with β_1 and β_2 given by (4.6) and (6.6), respectively.

the model at leading order. The resulting boundary conditions (2.12) capture the important physical effects of surfactant in a single dimensionless parameter E.

Through the method of matched asymptotic expansions, we derive results for the dimensionless height of the thin films between the bubble and the channel walls and for the corrections to the pressure drop across the front and rear menisci of the bubble. Such an analysis is reliant on the bubble being long, so we can treat the front and rear of the bubble separately. Our bulk equilibrium surfactant model produces results analogous to Bretherton's, in which the thin film height and the pressure corrections scale with $Ca^{2/3}$ (Bretherton 1961), but where the prefactors are now numerically determined functions of E, with the surfactant-free case corresponding to E=0. Previous work (Waters & Grotberg 2002) found that the height of the deposited film is a decreasing function of E in the limit $E \to 0$. Strikingly, we show that this asymptotic prediction fails for E as small as 0.2, and in fact the film height almost always increases with E, up to a maximum value larger than Bretherton's by a factor of $4^{2/3}$. Likewise, we find that the net pressure difference across both menisci increases with E, again by a factor of up to $4^{2/3}$ in the limit as $E \to \infty$. The factor of $4^{2/3}$ comes from the bubble surface being stationary in the lab frame of reference, rather than satisfying the zero-stress condition as in the original Bretherton problem.

The key outputs from our analysis are the normalised corrections to the pressure drop β_1 and β_2 across the front and rear meniscus, respectively. In practice, the computation of these parameters across a range of values of E is very challenging because of the extreme sensitivity of the relevant shooting problems, especially for the rear meniscus, where there are two shooting parameters. To perform an exhaustive parameter sweep, particularly in the singular limit where $E \to 0$, it may be necessary to adopt an alternative numerical approach, for example solving the boundary-value problem directly by discretizing the whole domain.

We use our results for the modified pressure drop across the bubble to obtain a generalised equation of motion for a bubble in a Hele-Shaw cell that includes the effects of surfactants. As in Booth *et al.* (2023), the effective viscous drag on the bubble is measured by a dimensionless "Bretherton parameter" $\delta \propto \text{Ca}^{1/3}/\epsilon$, with just the prefactor now a function of E (see (7.2)). We find that, for the same flow conditions, an isolated surfactant-laden bubble will travel more slowly than an isolated surfactant-free bubble. Crucially, E depends only on the physical

properties of the surfactant and the fluid, as well the cell height, but not on any local flow properties (e.g., the local capillary number). The model thus easily generalises to an arbitrary number of bubbles by modifying the prefactor in δ in the same way for each bubble.

Our modelling relies on the surfactant being highly soluble, in the sense that the timescale for adsorption is much shorter than that for surfactant transport, i.e., the Damköhler number is large. It also relies on the capillary number being small, i.e., the bubble propagates slowly enough for the free surface to be dominated by capillary effects. The former can be achieved in practice using surfactants such as sodium alkyl sulphates, or alkyl trimethylammonium bromides with fewer than 11 carbons in the alkyl chain (Baué *et al.* 2025). The latter is almost always satisfied in microfluidic devices (Stone *et al.* 2004).

Our analysis relies on the front and rear menisci being well separated in the flow direction, which is not true near the "poles" of the bubble (in plane view), where the bubble meniscus is parallel to the background velocity. In these regions, a different asymptotic scaling allows one to explain how the parameter β varies smoothly between the constant values β_1 and β_2 , as shown by Burgess & Foster (1990) for clean bubbles. However, Booth *et al.* (2023) showed that these regions provide a correction to the bubble velocity that is $O(\epsilon^{6/5})$, and thus negligible to lowest order.

- Funding. DJB is grateful to EPSRC, grant reference number EP/V520202/1, for funding and is now funded as
 part of the Leverhulme Trust Leadership Award 'Shape-Transforming Active Microfluidics' (RL-2019-014)
- 633 to Tom Montenegro-Johnson at the University of Warwick
- 634 **Declaration of interests.** The authors report no conflict of interest.

REFERENCES

- BAUÉ, J.-T., GANS, A., JANNIN, L., REICHERT, B., CANTAT, I. & JULLIEN, M.-C. 2025 Droplet velocity in both limits of low and high soluble surfactants in a hele-shaw cell: experimental and analytical results. *J. Fluid Mech.* 1009, A23.
- BOOTH, D.J., GRIFFITHS, I.M. & HOWELL, P.D. 2023 Circular bubbles in a Hele-Shaw channel: a Hele-Shaw
 Newton's cradle. *J. Fluid Mech.* 954, A21.
- BOOTH, D.J., GRIFFITHS, I.M. & HOWELL, P.D. 2025a The motion of a bubble in a non-uniform flow. *Proc.* Roy. Soc. A 481 (2311), 20240613.
- BOOTH, D.J., Wu, K., GRIFFITHS, I.M., HOWELL, P.D., NUNES, J.K. & STONE, H.A. 2025b Bubble racing in
 a Hele-Shaw cell. *J. Fluid Mech.* 1010, A19.
- 644 Bretherton, F. 1961 The motion of long bubbles in tubes. J. Fluid Mech. 10 (2), 166–188.
- Burgess, D. & Foster, M.R. 1990 Analysis of the boundary conditions for a Hele-Shaw bubble. *Phys. Fluids A* 2 (7), 1105–1117.
- DELACOTTE, J., MONTEL, L., RESTAGNO, F., SCHEID, B., DOLLET, B., STONE, H.A., LANGEVIN, D. & RIO, E. 2012 Plate coating: influence of concentrated surfactants on the film thickness. *Langmuir* **28** (8), 3821–3830.
- 650 FUJIOKA, H. & GROTBERG, J.B. 2005 The steady propagation of a surfactant-laden liquid plug in a two-651 dimensional channel. *Phys. Fluids* **17** (8), 082102.
- GHADIALI, S.N. & GAVER, D.P. 2003 The influence of non-equilibrium surfactant dynamics on the flow of a semi-infinite bubble in a rigid cylindrical capillary tube. *J. Fluid Mech.* **478**, 165–196.
- 654 GINLEY, G.M. & RADKE, C.J. 1989 Influence of soluble surfactants on the flow of long bubbles through a cylindrical capillary. *ACS Symp. Ser.* **396**, 480–501.
- GOUNLEY, J, BOEDEC, G, JAEGER, MARC & LEONETTI, M 2016 Influence of surface viscosity on droplets in
 shear flow. J. Fluid Mech. 791, 464–494.
- 658 Grotberg, J.B. 2011 Respiratory fluid mechanics. Phys. Fluids 23 (2).
- HALPERN, D. & GAVER, D.P. 2012 The influence of surfactant on the propagation of a semi-infinite bubble through a liquid-filled compliant channel. *J. Fluid Mech.* **698**, 125–159.
- MARUVADA, S.R.K. & PARK, C.-W. 1996 Retarded motion of bubbles in Hele-Shaw cells. *Phys. Fluids* **8** (12), 3229–3233.

- Muradoglu, M., Romanò, F., Fujioka, H. & Grotberg, J.B. 2019 Effects of surfactant on propagation and rupture of a liquid plug in a tube. *J. Fluid Mech.* 872, 407–437.
- Park, C.-W. 1992 Influence of soluble surfactants on the motion of a finite bubble in a capillary tube. *Phys. Fluids A* **4** (11), 2335–2347.
- Park, C.-W. & Homsy, G.M. 1984 Two-phase displacement in Hele-Shaw cells: theory. *J. Fluid Mech.* **139**, 291–308.
- Park, C.-W., Maruvada, S.R.K. & Yoon, D.-Y. 1994 The influence of surfactant on the bubble motion in Hele-Shaw cells. *Phys. Fluids* **6** (10), 3267–3275.
- RATULOWSKI, J. & CHANG, H.-C. 1990 Marangoni effects of trace impurities on the motion of long gas bubbles in capillaries. *J. Fluid Mech.* **210**, 303–328.
- 673 SHEMILT, J.D., HORSLEY, A., JENSEN, O.E., THOMPSON, A.B. & WHITFIELD, C.A. 2023 Surfactant amplifies 674 yield-stress effects in the capillary instability of a film coating a tube. *J. Fluid Mech.* **971**, A24.
- 675 Shen, A.Q., Gleason, B., McKinley, G.H. & Stone, H.A. 2002 Fiber coating with surfactant solutions.
 676 Phys. Fluids 14 (11), 4055–4068.
- STEBE, K.J. & BARTHES-BIESEL, D. 1995 Marangoni effects of adsorption—desorption controlled surfactants on the leading end of an infinitely long bubble in a capillary. *J. Fluid Mech.* **286**, 25–48.
- Stone, H.A. 1990 A simple derivation of the time-dependent convective-diffusion equation for surfactant transport along a deforming interface. *Phys. Fluids A* **2** (1), 111–112.
- Stone, H. A., Stroock, A. D. & Ajdari, A. 2004 Engineering flows in small devices: microfluidics toward a lab-on-a-chip. *Annu. Rev. Fluid Mech.* **36** (1), 381–411.
- Taylor, G. & Saffman, P.G. 1959 A note on the motion of bubbles in a Hele-Shaw cell and porous medium. *Q. J. Mech. Appl. Math.* 12 (3), 265–279.
- WATERS, S.L. & GROTBERG, J.B. 2002 The propagation of a surfactant laden liquid plug in a capillary tube.

 Phys. Fluids 14 (2), 471–480.
- Wu, K., Booth, D.J., Griffiths, I.M., Howell, P.D., Nunes, J.K. & Stone, H.A. 2024 The motion and deformation of a bubble in a Hele-Shaw cell. *Phys. Rev. Fluids* **9** (12), 123603.
- ZHENG, Y., FUJIOKA, H. & GROTBERG, J. B. 2007 Effects of gravity, inertia, and surfactant on steady plug propagation in a two-dimensional channel. *Phys. Fluids* **19** (8).